Available online at www.ijournalse.org

Emerging Science Journal

(ISSN: 2610-9182)

Vol. 9, No. 6, December, 2025

Enhanced Optimization Strategy to Maximize Achievable Rate of Millimeter-Wave Full-Duplex UAV on Multiple User

Dwi Harinitha [1, 2*], Irma Zakia [1*], Iskandar [1]

[1] *School of Electrical Engineering and Informatics, Institut Teknologi Bandung, Bandung, 40132, Indonesia.*

[2] *Department of Electrical Engineering, Faculty of Engineering, Institut Teknologi Padang, Padang 25143, Indonesia.*

Abstract

This study proposes an enhanced optimization strategy to maximize the achievable data rate of millimeter-wave (mmWave) full-duplex (FD) unmanned aerial vehicles (UAVs) in multi-user scenarios. The objective is to address signal degradation from high-frequency path loss and self-interference while ensuring efficient resource allocation across multiple user equipment (UEs). A joint optimization framework is introduced, integrating UAV positioning, beamforming vector design at both the gateway and UAV, and power allocation. Initially, the Alternating Interference Suppression (AIS) algorithm is adapted for multiple UEs, but due to emerging non-convexity, the problem is reformulated using a first-order approximation approach. The solution is decomposed into two iterative sub-problems—optimizing UAV location and then solving for beamforming and power distribution. MATLAB-based simulations validate the proposed approach, revealing a threefold increase in achievable data rate and a 40.85% improvement in power efficiency compared to non-optimized systems. The novelty of this work lies in its scalable multi-user adaptation and its integrated, power-aware optimization algorithm, outperforming conventional FD and half-duplex strategies. This contribution significantly advances the design of efficient, high-throughput UAV communication systems for next-generation wireless networks, especially in environments with frequent line-of-sight obstructions.

Keywords:

Bit Rate;
Full-Duplex;
Jointly Optimization;
mmWave;
First-Order Approximation.

Article History:

Received:	14	April	2025
Revised:	11	August	2025
Accepted:	07	September	2025
Published:	01	December	2025

1- Introduction

New generation cellular communication system includes advanced high-speed broadband capabilities, providing a promising opportunity for the mmWave communication system to be widely implemented in the future [1-3]. However, wavelength and attenuation issues require extensive study to improve the performance [4, 5]. The large attenuation issue and penetration losses appear due to its high frequency, harmful diffraction of the electromagnetic waves, and complex environment [6, 7]. Therefore, mmWave signal propagation with a smaller wavelength will be blocked by the object size in the environment. For the reason above, the alternative multipath component is required to help propagation, where line of sight (LOS) decides the successful transmission of the mmWave signal [8-10].

The emergence of alternative communication systems in the form of aviation platforms, such as high-altitude platforms (HAPs) and unmanned aerial vehicles (UAVs), can be employed as aerial base stations (BS) to enhance transmission system performance and establish temporary communication [11-14]. This platform will provide fairly wide coverage and availability of LOS communication, as well as reduced development, infrastructure, and implementation costs. Meanwhile, the mmWave high path loss can be addressed by the full-duplex (FD) technique. It

* **CONTACT**: irma.zakia@itb.ac.id; dwiharinitha@itp.ac.id

DOI: http://dx.doi.org/10.28991/ESJ-2025-09-06-07

will improve the data rate with transmissions and receptions simultaneously in the same frequency band. Furthermore, the leaked transmit signal from the transmitter to the receiver node is known as self-interference (SI). It influences the very noisy received signal and renders decoding the desired signal impossible [15-17]. Therefore, SI is suppressed below the level of the receiver noise floor to achieve more advantage of FD communication [18, 19].

Existing research on improving joint optimization for UAV communications has been studied. Research by Yang et al. [20], and Andreou et al. [21] presents an approach to minimize total uplink power while meeting minimum user data rate demands. This is achieved by jointly optimizing the UAV flying height, antenna beamwidth, UAV location, ground terminal bandwidth allocation, and transmit power. Previous studies show that total power and energy consumption in a mobile edge computing (MEC) network can be minimized by jointly optimizing UAV location, power control, computing capacity allocation, and location planning [22–24]. The goal of maximizing the total effective capacity for all users in the downlink is addressed in research by Niu et al. [25] through the joint optimization of the UAV's 3D location, power, and bandwidth allocation, while taking into account each user's statistical quality of service (QoS) requirements. The aim to minimize transmission delays between UAVs and ground users through the optimization of UAV location, user transmit power, and bandwidth allocation for each user is addressed in research by Xu et al. [26]. An optimization problem was proposed and formulated to maximize the minimum signal-to-interference-plus-noise ratio (SINR) for users by determining the optimal power allocation and UAV locations [27-29].

Extensive research has focused on mmWave frequency bands for UAV communications, driven by their impressive ability to provide both reliable and adaptable connections [30]. Current research emphasizes improving the data rates of mmWave full-duplex aerial systems. For example, Harinitha et al. [31] demonstrated that the data rate for each user equipment (UE) from a high-altitude platform (HAP) is affected by the distance between the HAP and the UE, highlighting the importance of optimal HAP positioning. Additionally, Liu et al. [32], and Hashir et al. [33] improved the rate of the source-to-UAV and UAV-to-destination links by jointly optimizing UAV positioning, analog beamforming, and power control.

Recent research has focused on maximizing the achievable rate of millimeter-wave (mmWave) full-duplex (FD) UAV systems. These studies explore joint optimization of UAV positioning, beamforming, and power control to enhance communication capacity [1, 34]. The use of large antenna arrays helps mitigate high path loss and self-interference in mmWave channels [34, 35]. Some researchers have investigated the impact of specific mmWave carrier frequencies on system performance, considering factors such as residual self-interference, bandwidth, and UAV altitude [36]. Multi-objective optimization frameworks have been proposed to maximize both uplink and downlink rates while ensuring quality-of-service for multiple users [33]. These studies consistently demonstrate that FD-UAV systems outperform traditional half-duplex systems in mmWave communications [33, 34]. However, challenges remain in addressing the high non-convexity of optimization problems and the performance degradation caused by increased frequency, distance, and UAV altitude in mmWave communications [36, 37]. Despite these advancements, most existing studies either focus on single-user scenarios or do not fully exploit the joint optimization of UAV positioning, beamforming, and power allocation in a multi-user FD mmWave network. The interaction and coupling between these variables across multiple users introduce complex, highly non-convex problems that remain insufficiently addressed. A comprehensive approach that can handle these challenges while maximizing both uplink and downlink rates in multi-user environments is still lacking.

A multi-objective optimization framework for sum uplink and downlink rate maximization in an FD-UAV network was proposed by Hashir et al. [33]. A joint optimization of UAV relay positioning, hybrid beamforming, and power allocation maximizes the achievable rate in a multi-user massive MIMO IoT system with millimeter-wave communications [38]. A joint optimization of TDMA-based user scheduling, UAV trajectory, and transmit power maximizes the achievable rate of a full-duplex UAV relaying network for multiple user pairs [39].

Building on the work of Zhu et al. [34], this paper expands scenario from a single-user to a multi-user, focusing on reformulating the resource allocation problem to maximize the end-to-end data rate in a network with multiple UEs. The reformulated problem introduces additional challenges due to its nonconvex nature and the coupling of variables between different users. To address this, first-order approximation is developed to maximize the achievable rate in the downlink direction of mmWave FD UAVs for multi-user scenarios. The problem is decomposed into two subproblems, resulting in an iterative maximization of the end-to-end achievable rate. Specifically, the UAV position is optimized first, followed by the design of optimal beamforming vectors at the gateway and UAV, as well as the transmitted power for each UE. The proposed solution significantly increases the achievable rate compared to approaches that do not optimize the UAV position, beamforming vectors, or transmitted power. By addressing the critical interactions between these variables in a multi-user environment, the proposed solution significantly improves the achievable rate compared to conventional approaches that treat these parameters in isolation. Furthermore, the framework ensures efficient power usage by avoiding unnecessary transmission power while maintaining fairness through minimum rate guarantees for all users.

This paper introduces an improved UAV relay system designed to optimize achievable data rates along the ground link path, specifically within a multi-UE context. The research improves the works of Zhu et al. [34], from a single-user

to a multi-user scenario in the context of resource allocation. The goal is to maximize the minimum achievable data rate without wasting power when multiple UEs are present in the network. Therefore, a novel optimization is introduced to maximize the uplink (backhaul link) and downlink (access link) achievable rate for mmWave FD UAVs in a multi-user environment. The research begins by optimizing the UAV's position, subsequently advancing to the design of beamforming and power allocation to ensure optimal power usage. Unlike most prior studies that focus on single-user scenarios or only optimize a subset of variables (e.g., UAV position, beamforming, or power allocation), this work presents a comprehensive joint optimization framework for a multi-user mmWave full-duplex UAV relay system. By addressing the coupling between UAV positioning, beamforming vectors, and power allocation across multiple users, our approach provides a more practical and efficient solution for maximizing end-to-end data rates while ensuring fairness and power efficiency.

The structure of this paper consists of four sections, as follows: Section 1 serves as the introductory section and provides background information for the study. Section 2 outlines the proposed system model, detailing the channel models and problem formulation. Section 3 delves into the optimization strategies, including UAV positioning, beamforming design, and power allocation. Section 4 provides the simulation results along with an in-depth discussion. Lastly, Section 5 concludes with final remarks.

2- System Model

Figure 1 shows the flow of proposed research begins by initializing all system parameters, including UAV altitude bounds, user locations, power constraints, and initial values for position, beamforming, and power allocation. The first major step is to determine the UAV's optimal 3D position to enhance line-of-sight connectivity and minimize path loss. Once positioned, the beamforming vectors at both the UAV and gateway are designed. Due to the non-convex nature of the problem—particularly the quadratic components in the beamforming formulation—a first-order approximation technique is employed to linearize and resolve these components, making the optimization tractable. Following this, optimal power allocation is performed to ensure efficient transmission, aiming to maximize the achievable data rate across all users without exceeding power constraints. Finally, the results are analyzed in terms of system performance metrics such as end-to-end data rate, convergence behavior, and power efficiency, concluding the iterative optimization process.

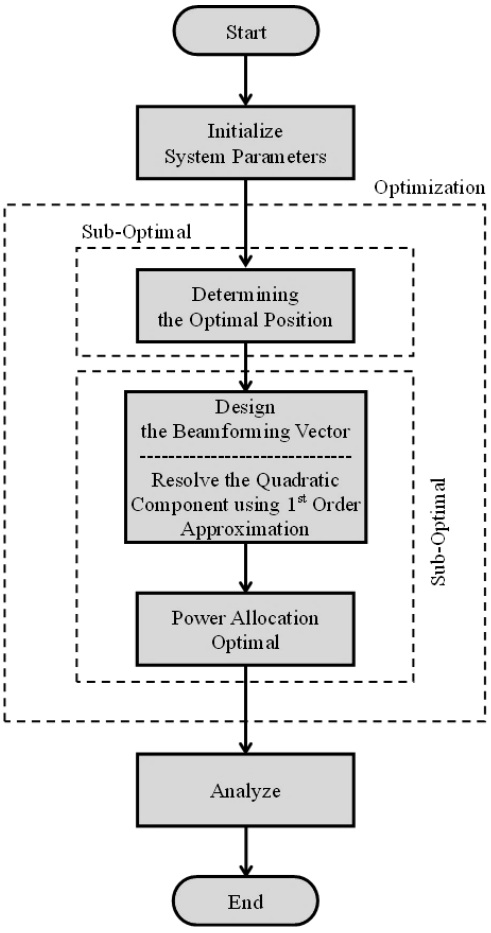

Figure 1. Flowchart of methodology

2-1- Channel Models

This section presents the channel model and problem formulation of maximizing the end-to-end achievable rate by jointly optimizing UAV position, beamforming vectors, and power allocation. The scenarios for UAV communication are illustrated in Figure 2. The G2V, V2U$_k$, and G2U$_k$ are the links from gateway to UAV (uplink), UAV to k^{th} UE (downlink), and gateway to k^{th} UE (ground link), respectively. Where, $k = 1, 2, \ldots, K$ is the number of UEs. The presence of G2V and V2U$_k$ links, predominantly comprising LOS connections with an estimated flat-fading channel model, is designed to facilitate obstructed transmissions from G2U$_k$. Consequently, the calculation of achievable rates on the G2U$_k$ link is executed by maximizing the rates achievable on the G2V and V2U$_k$ links.

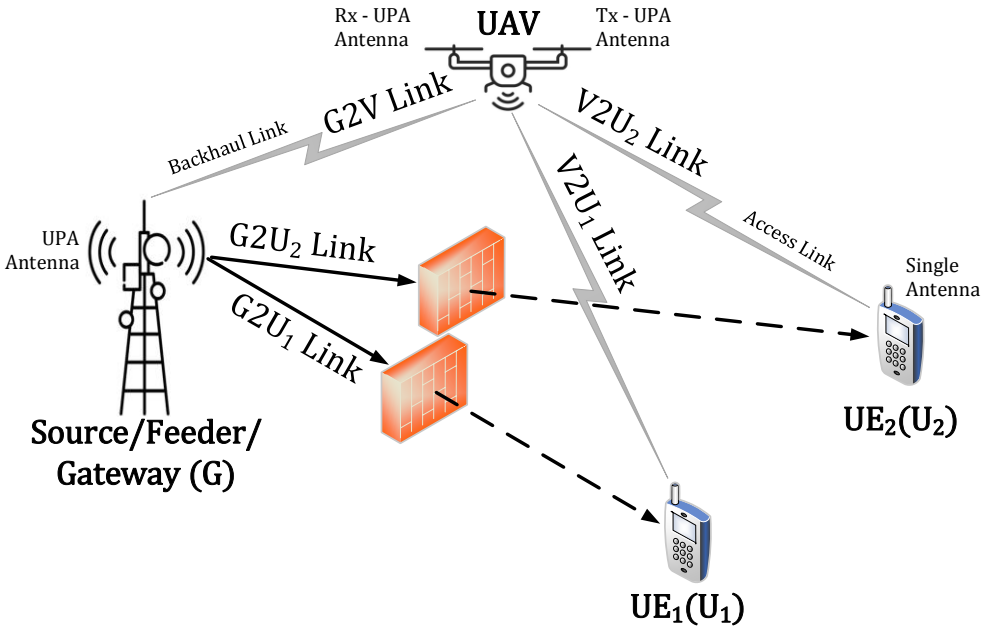

Figure 2. UAV communications scenario for k = 2

The channel model includes two parts: G2V and V2U$_k$. Each part can be either in LOS or Non-Line-of-Sight (NLOS) conditions. Additionally, the channel from the gateway to the user equipments (UEs), denoted as G2U$_k$, is typically considered NLOS. Referring to the channel matrix presented in Zhu et al. [34], it is commonly expressed as

$$\boldsymbol{H}_{Link} = \overbrace{\chi_{Link}\beta_{Link}^{(0)}\boldsymbol{a}_\tau\left(\theta_\tau^{(0)},\phi_\tau^{(0)}\right)\boldsymbol{a}_\tau^H\left(\theta_\tau^{(0)},\phi_\tau^{(0)}\right)}^{LOS\ path} + \overbrace{\sum_{\ell=1}^{L_{Link}}\beta_{Link}^{(\ell)}\boldsymbol{a}_\tau\left(\theta_\tau^{(\ell)},\phi_\tau^{(\ell)}\right)\boldsymbol{a}_\tau^H\left(\theta_\tau^{(\ell)},\phi_\tau^{(\ell)}\right)}^{NLOS\ path} \quad (1)$$

where $(\cdot)_{Link}$ represents the G2V, V2U$_k$, and G2U$_k$ links. H_{Link} is the channel matrix $Link$. χ_{Link} is the LOS/NLOS random variable $Link$ that will take the value 1 if there is an LOS path. The complex coefficients $Link$ for LOS and NLOS conditions are denoted as $\beta_{Link}^{(0)}$ and $\beta_{Link}^{(\ell)}$, respectively. 0 indicates LOS, and ℓ indicates NLOS. These coefficients are influenced by the link distance parameters and the operating frequency. The distance parameters depend on the positions of the UAV relative to the gateway, the UAV relative to the UE$_k$ and the gateway relative to the UE$_k$, considering the coordinates on the x-axis, y-axis, and h-altitude (x, y, h).

Furthermore, the vector $\boldsymbol{a}_\tau\left(\theta_\tau^{(\ell)},\phi_\tau^{(\ell)}\right)$ represents the uniform planar array (UPA) antenna steering vector, as described in Zakia [40]. The UPA antenna is used for realizing transmit beamforming at the gateway $\boldsymbol{a}_G$, as well as received $\boldsymbol{a}_r$ and transmit beamforming $\boldsymbol{a}_{t_k}$ at the UAV. For simplicity, we generalize these steering vectors as $\boldsymbol{a}_\tau$, where τ represents the gateway (G), receiver (r), and k^{th} transmitter (t_k), thereby $\tau = \{G, r, t_k\}$. The variables $\theta_\tau^{(\ell)}$ and $\phi_\tau^{(\ell)}$ are the elevation and azimuth angles, respectively, which are in the range $[-\pi/2, \pi/2]$ and $[-\pi, \pi]$. $(\cdot)^H$ represents the Hermitian indicator. The UEs are equipped with a single antenna. Therefore, the channel models of the G2V, V2U$_k$, and G2U$_k$ links are represented as follows:

$$\boldsymbol{H}_{G2V} = \chi_{G2V}\beta_{G2V}^{(0)}\boldsymbol{a}_r\left(\theta_r^{(0)},\phi_r^{(0)}\right)\boldsymbol{a}_G^H\left(\theta_G^{(0)},\phi_G^{(0)}\right) + \sum_{\ell=1}^{L_{G2V}}\beta_{G2V}^{(\ell)}\boldsymbol{a}_r\left(\theta_r^{(\ell)},\phi_r^{(\ell)}\right)\boldsymbol{a}_G^H\left(\theta_G^{(\ell)},\phi_G^{(\ell)}\right) \quad (2)$$

$$\boldsymbol{h}_{V2U_k} = \chi_{V2U_k}\beta_{V2U_k}^{(0)}\boldsymbol{a}_{t_k}^H\left(\theta_{t_k}^{(0)},\phi_{t_k}^{(0)}\right) + \sum_{\ell=1}^{L_{V2U_k}}\beta_{V2U_k}^{(\ell)}\boldsymbol{a}_{t_k}^H\left(\theta_{t_k}^{(\ell)},\phi_{t_k}^{(\ell)}\right) \quad (3)$$

$$\boldsymbol{h}_{G2U_k} = \sum_{\ell=1}^{L_{G2U_k}}\beta_{G2U_k}^{(\ell)}\boldsymbol{a}_G^H\left(\theta_{\tilde{G}}^{(\ell)},\phi_{\tilde{G}}^{(\ell)}\right) \quad (4)$$

The G2V channel model is a channel matrix (denoted as $\boldsymbol{H}_{G2V}$) represented by a 16×16 matrix, whereas the sizes of the V2U$_k$ and G2U$_k$ channels, which are channel vectors (denoted as $\boldsymbol{h}_{V2U_k}$ and $\boldsymbol{h}_{G2U_k}$), are 16×1 vectors, all of which are complex-valued. The SI channel is modelled using the near-far model, as described in Zhang et al. [18], and Zhu et al. [34];

$$[\boldsymbol{H}_{SI}]_{m,n} = \beta_{SI}^{(m,n)} exp\left(-j2\pi \frac{r_{m,n}}{\lambda}\right) \tag{5}$$

where $\beta_{SI}^{(m,n)}$ is the complex coefficient of the SI channel, λ is the wavelength, and $r_{m,n}$ pertains to the distance between the m^{th} element of transmitting array and the n^{th} element of the receiving array.

2-2- Problem Formulation

An essential aspect of data communication pertains to the rate at which data is transmitted through the communication channel. As a result, the optimization of the achievable rate along the end-to-end link becomes imperative when the UAV processes the backhaul signal received from the gateway and subsequently relays it to each UE. The goal of this research is to achieved power-saving transmission and maximize the end-to-end achievable rate when the UAV receives a backhaul signal from the gateway and then transmits it to multiple UE. The achievable rate is typically defined as follows:

$$R = log_2(1 + SINR_{Link}) \tag{6}$$

where the SINR is calculated assuming perfect knowledge of the fading channel at the receiver. The G2V link serves as a wireless backhaul, and its capacity plays a crucial role in determining the achievable data transmission rate for the UE. The achievable rates for the G2V and V2U$_k$ links are

$$R_{G2V} = log_2(1 + SINR_{G2V}) \tag{7}$$

and

$$R_{V2U_k} = log_2\left(1 + SINR_{V2U_k}\right) \tag{8}$$

$$R_{V2U_{tot}} = \sum_{k=1}^{K} R_{V2U_k} \tag{9}$$

Beamforming can significantly enhance the SINR by focusing the signal energy towards the UE and reducing interference. This improvement in SINR enables the use of higher modulation schemes, resulting in an increased achievable data rate from the gateway to the user equipment. Mathematically, the SINR for the G2V link can be formulated as;

$$SINR_{G2V} = \frac{\left|\boldsymbol{w}_r^H \boldsymbol{H}_{G2V} \boldsymbol{w}_G\right|^2 P_G}{\left|\boldsymbol{w}_r^H \boldsymbol{H}_{SI} \boldsymbol{w}_t\right|^2 P_V + \sigma_V^2} \tag{10}$$

and the SINR for the V2U$_k$ link is defined as

$$SINR_{V2U_k} = \frac{\left|\boldsymbol{w}_U^H \boldsymbol{H}_{V2U} \boldsymbol{w}_t\right|^2 P_V}{\left|\boldsymbol{w}_U^H \boldsymbol{H}_{G2U} \boldsymbol{w}_G\right|^2 P_G + \sigma_U^2} \tag{11}$$

where $\boldsymbol{w}_r, \boldsymbol{w}_G, \boldsymbol{w}_t, \boldsymbol{w}_U$ denotes the beamforming vector at receiver, gateway, transmitter, and UE, respectively. P_G and P_V denote the transmitted powers from the gateway and UAV respectively. Moreover, σ_V^2 denotes noise power levels on the UAV and σ_U^2 indicates noise power levels on the UE. In case of multiple UE, a P_V for each UE denoted as P_{V_k}, and σ_U^2 at each UE denoted as σ_{Uk}^2. The total achievable rate for G2U and V2U denoted as G2U$_{tot}$ and V2U$_{tot}$, respectively.

The end-to-end achievable rates of G2U$_{tot}$ are determined by computing the minimum value between the achievable rate of G2V and the sum of all V2U links, as expressed below:

$$R_{G2U_{tot}} = min\{R_{G2V}, R_{V2U_{tot}}\} \tag{12}$$

Finally, the problem formulation is

$$\begin{aligned} \max_{x,y,h,\boldsymbol{w}_\tau,P_G,P_{V_k}} \quad & min\{R_{G2V}, R_{V2U_{tot}}\} \\ s.t. \quad & (x,y) \in [0, x_{U_k}] \times [0, y_{U_k}] \\ & h_{min} \le h \le h_{max} \\ & |[\boldsymbol{w}_\tau]_n| \le \frac{1}{\sqrt{N_\tau^{tot}}}, \ \forall n, \\ & 0 \le P_G \le 0 \\ & 0 \le P_{V_k} \le 0 \end{aligned} \tag{13}$$

where; x_{U_k} and y_{U_k} represent the *x*-axis and *y*-axis coordinates of the k^{th} UE, respectively. The minimum and maximum altitudes of the UAV are represented by the variables h_{min} and h_{max}, respectively. N_τ^{tot} is equal to $M_\tau \times N_\tau$ for the UPA antenna. On the other hand, $[\boldsymbol{w}_\tau]_n$ represents constant-modulus on the beamforming vectors.

The objective function is nonconvex, and the variables $\{x, y, h, \boldsymbol{w}, P\}$ are coupled. To simplify the problem, we decompose it into smaller subproblems. This is done by optimizing one variable at a time while keeping the others fixed, as suggested in Palomar & Chiang [41]. We start by determining the optimal positions for the UAV (*x*, *y*, and *h*), and then proceed to optimize the beamforming vectors and transmit power allocation. Optimizing UAV placement and signal processing parameters directly impacts real-world applications such as:

- Disaster recovery communication: Ensuring connectivity in areas with damaged infrastructure.
- Rural and remote connectivity: Enhancing access in underserved regions.
- Emergency and military networks: Providing reliable communication for field operations.

3- Optimization

3-1- Positioning

The probability of LOS conditions increases with the altitude in a UAV communication system. Therefore, the UAV's position is crucial. As discussed in Zhu et al. [34], optimizing the UAV's position involves several assumptions, such as a LOS environment, ideal beamforming, and the suppression of SI and interference from G2U link. The achievable rate under LOS conditions and ideal beamforming is influenced by factors such as the G2V distance, V2U distance, and the transmit power of both the gateway and the UAV. The calculated achievable rate represents the upper bound for LOS conditions. The rate obtained is a strict upper bound if NLOS conditions are also considered.

In UAV-assisted communication systems, the probability of LOS conditions increases significantly with UAV altitude, due to reduced likelihood of obstacles in the propagation path [42, 43]. As such, optimizing the UAV's position under the assumption of LOS conditions is reasonable and allows us to establish an upper bound on system performance. To simplify analysis, we also assume ideal beamforming, which is a common practice in upper-bound analyses of UAV-enabled communication systems [44, 45]. While real-world systems experience beamforming errors and misalignments, these effects are omitted here to focus on spatial optimization. Lastly, we assume effective suppression of self-interference (SI) and interference from the G2U link. This is motivated by the progress in full-duplex communication and interference mitigation technologies [46, 47]. While perfect suppression is not always achievable in practice, our assumption enables analytical tractability.

The solution for determining the optimal UAV position starts with mathematically finding the points on the *x*-axis and *y*-axis. Then, the altitude is chosen within 100 to 300 meters above ground level, considering the probability of a LOS connection. The probabilities of a LOS path existing for the G2V and V2U links are modelled as functions of the elevation angles and positive modelling parameters [34, 48] can be expressed as follows:

$$P_{G2V}^{LOS} = \frac{1}{1+a\ exp\left(-b\left(\frac{180}{\pi}\theta_r^{(0)}-a\right)\right)} \tag{14}$$

and

$$P_{V2U_k}^{LOS} = \frac{1}{1+a\ exp\left(-b\left(\frac{180}{\pi}\theta_{t_k}^{(0)}-a\right)\right)} \tag{15}$$

The values of the positive modelling parameters, *a* and *b*, are dictated by the propagation environment. Multiple iterations (*i*) are conducted in a MATLAB simulation to determine the most advantageous location. This process aims to achieve the highest LOS probability with the shortest UAV movement. The optimal position is mathematically expressed as follows [34]:

$$(x^\star, y^\star, h^\star) = \arg\min_{(x,y,h)} d_{x,y,h} \tag{16}$$

where $(\cdot)^\star$ represents the optimal value/condition and $d_{x,y,h}$ is a distance of UAV displacement/shift from the initial position.

3-2- Beamforming Design and Power Allocation

The subsequent stage after obtaining the optimal position is to design the beamforming vector (BFV) considering various environmental factors such as LOS and NLOS. Consequently, the alternating interference suppression (AIS) algorithm, which was introduced in Zhu et al. [34], is implemented to mitigate the complexity of beamforming optimization. Unlike the approach in Zhu et al. [34], where the SINR formulation exclusively focuses on single users,

this study employs a multi-user perspective. This reveals that the denominator in Equations 10 and 11 accounts for the collective number of users. A significant disparity is evident in Equation 11, specifically in the computation of SINR for the V2U$_k$ link. Here, the denominator is affected by both the G2U$_k$ channel and the channels of neighboring V2U$_k$, impact to reducing achievable rate and increasing the complexity of the calculations. SINR on a G2V link for multi users in this research is defined as:

$$SINR_{G2V} = \frac{\left|\boldsymbol{w}_r^H \boldsymbol{H}_{G2V} \boldsymbol{w}_G\right|^2 P_G}{\sum_{k=1}^{K} \left|\boldsymbol{w}_r^H \boldsymbol{H}_{SI} \boldsymbol{w}_{t_k}\right|^2 P_{V_k} + \sigma_V^2} \tag{17}$$

Meanwhile SINR for the V2U$_k$ link is defined as:

$$SINR_{V2U_k} = \frac{\left|\boldsymbol{h}_{V2U_k}^H \boldsymbol{w}_{t_k}\right|^2 P_{V_k}}{\left(\left|\boldsymbol{h}_{G2U_k}^H \boldsymbol{w}_G\right|^2 P_G\right) + \left(\sum_{\ell \neq k}^{K} \left|\boldsymbol{h}_{V2U_k}^H \boldsymbol{w}_{t_\ell}\right|^2 P_{V_\ell}\right) + \sigma_{Uk}^2} \tag{18}$$

The design process involves two steps: First step, initialize the BFV by normalizing the steering vector for the LOS conditions in both the G2V and V2U channels [34]. The second step involves an iterative procedure optimizes the BFVs $\boldsymbol{w}_r$, $\boldsymbol{w}_{t_k}$, and $\boldsymbol{w}_G$ through the suppression of SI, ultimately receive the maximum of signal strength. The BFV by normalizing the steering vector are:

$$\boldsymbol{w}_\tau^{(0)} = \frac{1}{\sqrt{N_\tau^{tot}}} \boldsymbol{a}_\tau\left(\theta_\tau^{(0)}, \phi_\tau^{(0)}\right) \tag{19}$$

The proposed iterative solution for Multiple-UE ($K = 2$) is generalized from the formula in Zhu et al. [34]. Due to multiple UEs, $R_{V2U_{tot}}$ represents the total achievable rate of all V2U links, as formulated in Equation 9. Mathematically, if the numerator is assumed to be a_k and the denominator b_k, then for K=2, the equation can be expressed as follows:

$$\begin{aligned} R_{V2U_{tot}} &= R_{V2U_1} + R_{V2U_2} \\ &= log_2\left(1 + \frac{a_1}{b_1}\right) + log_2\left(1 + \frac{a_2}{b_2}\right) \\ &= log_2\left(\left(1 + \frac{a_1}{b_1}\right)\left(1 + \frac{a_2}{b_2}\right)\right) \\ &= log_2\left(1 + \frac{a_1}{b_1} + \frac{a_2}{b_2} + \frac{a_1 a_2}{b_1 b_2}\right) \\ &= log_2\left(1 + \frac{(a_1 b_2)(a_2 b_1)(a_1 a_2)}{(b_1 b_2)}\right) \end{aligned} \tag{20}$$

Thus, the total SINR to be used for optimizing the beamforming vector (BFV) can be expressed as:

$$SINR_{V2U_{tot}} = \frac{A_1\left(A_6 + A_3 + \sigma_{U_2}^2\right) + A_4\left(A_5 + A_2 + \sigma_{U_1}^2\right) + (A_1 A_4)}{\left(A_6 + A_3 + \sigma_{U_2}^2\right)\left(A_5 + A_2 + \sigma_{U_1}^2\right)} \tag{21}$$

where $a_1 = A_1$, $a_2 = A_4$, $b_1 = A_5 + A_2 + \sigma_{U_1}^2$, $b_2 = A_6 + A_3 + \sigma_{U_2}^2$. Meanwhile, $A_1 = \boldsymbol{h}_{V2U_1}^H \boldsymbol{w}_{t_1}$, $A_2 = \boldsymbol{h}_{V2U_1}^H \boldsymbol{w}_{t_2}$, $A_3 = \boldsymbol{h}_{V2U_2}^H \boldsymbol{w}_{t_1}$, $A_4 = \boldsymbol{h}_{V2U_2}^H \boldsymbol{w}_{t_2}$, $A_5 = \boldsymbol{h}_{G2U_1}^H \boldsymbol{w}_G$, $A_6 = \boldsymbol{h}_{G2U_2}^H \boldsymbol{w}_G$. $A_1, \cdots, A_6$ is an auxiliary variable, while a_1, a_2, b_1, and b_2 are an expression built from auxiliary variables.

From a mathematical perspective, the formulas for both UEs can be expressed as shown in Equations 22 to 25. As observed for the multiple users, the limitations in those equations are distinct from those in Zhu et al. [34]. The coefficients that are affected by the number of users (k) need to be calculated, such as the BFV of each $\boldsymbol{w}_t$ $\left(\boldsymbol{w}_{t_k}\right)$ as in Equations 22 to 24 and the interfering channels from neighboring UEs ($\boldsymbol{h}_{V2U_k}$) in Equation 25.

$$\begin{aligned} &\underset{\boldsymbol{w}_r^{(i)}}{Maximize} \left|\boldsymbol{w}_r^{(i)H} \boldsymbol{H}_{G2V} \boldsymbol{w}_G^{(i-1)}\right| \\ &s.t \quad \left|\boldsymbol{w}_r^{(i)H} \boldsymbol{H}_{SI} \boldsymbol{w}_{t_1}^{(i-1)}\right| + \left|\boldsymbol{w}_r^{(i)H} \boldsymbol{H}_{SI} \boldsymbol{w}_{t_2}^{(i-1)}\right| \leq \eta_1^{(i)} \\ &\quad \left|\left[\boldsymbol{w}_r^{(i)}\right]_n\right| \leq \frac{1}{\sqrt{N_r^{tot}}}, \ 1 \leq n \leq N_r^{tot} \end{aligned} \tag{22}$$

$$\begin{aligned} &\underset{\boldsymbol{w}_{t_1}^{(i)}}{Maximize} \left|\mathrm{A}_1^{(i)}\right|\left|\mathrm{A}_6^{(i-1)}\right| + \left(\left|\mathrm{A}_1^{(i)}\right|\left|\mathrm{A}_3^{(i)}\right|\right) + \left|\mathrm{A}_1^{(i)}\right| + \left|\mathrm{A}_1^{(i)}\right|\left|\mathrm{A}_4^{(i)}\right| + \left|\mathrm{A}_5^{(i-1)}\right|\left|\mathrm{A}_4^{(i)}\right| + \left|\mathrm{A}_2^{(i)}\right|\left|\mathrm{A}_4^{(i)}\right| + \left|\mathrm{A}_4^{(i)}\right| \\ &s.t \quad \left|\boldsymbol{w}_r^{(i)H} \boldsymbol{H}_{SI} \boldsymbol{w}_{t_1}^{(i)}\right| + \left|\boldsymbol{w}_r^{(i)H} \boldsymbol{H}_{SI} \boldsymbol{w}_{t_2}^{(i-1)}\right| \leq \eta_{2_{t1}}^{(i)} \\ &\quad \left|\left[\boldsymbol{w}_{t_1}^{(i)}\right]_n\right| \leq \frac{1}{\sqrt{N_t^{tot}}}, \ 1 \leq n \leq N_t^{tot} \end{aligned} \tag{23}$$

$$\underset{\boldsymbol{w}_{t_2}^{(i)}}{Maximize}\ \left|\mathrm{A}_1^{(i)}\right|\left|\mathrm{A}_6^{(i-1)}\right| + \left|\mathrm{A}_1^{(i)}\right|\left|\mathrm{A}_3^{(i)}\right| + \left|\mathrm{A}_1^{(i)}\right| + \left|\mathrm{A}_1^{(i)}\right|\left|\mathrm{A}_4^{(i)}\right| + \left|\mathrm{A}_5^{(i-1)}\right|\left|\mathrm{A}_4^{(i)}\right| + \left(\left|\mathrm{A}_2^{(i)}\right|\left|\mathrm{A}_4^{(i)}\right|\right) + \left|\mathrm{A}_4^{(i)}\right|$$

$$s.t \quad \left|\boldsymbol{w}_r^{(i)H}\boldsymbol{H}_{SI}\boldsymbol{w}_{t_1}^{(i)}\right| + \left|\boldsymbol{w}_r^{(i)H}\boldsymbol{H}_{SI}\boldsymbol{w}_{t_2}^{(i)}\right| \le \eta_{2t_2}^{(i)} \tag{24}$$

$$\left|\left[\boldsymbol{w}_{t_2}^{(i)}\right]_n\right| \le \frac{1}{\sqrt{N_t^{tot}}},\ 1 \le n \le N_t^{tot}$$

$$\underset{\mathbf{w}_G^{(i)}}{Maximize}\ \left|\boldsymbol{w}_r^{(i)H}\boldsymbol{H}_{G2V}\boldsymbol{w}_G^{(i)}\right|$$

$$s.t \quad \left(\left|\mathrm{A}_5^{(i)}\right|\left|\mathrm{A}_6^{(i)}\right|\right) + \left|\mathrm{A}_5^{(i)}\right|\left|\mathrm{A}_3^{(i)}\right| + \left|\mathrm{A}_1^{(i)}\right| + \left|\mathrm{A}_6^{(i)}\right|\left|\mathrm{A}_2^{(i)}\right| + \left|\mathrm{A}_2^{(i)}\right|\left|\mathrm{A}_3^{(i)}\right| + \left|\mathrm{A}_2^{(i)}\right| + \left|\mathrm{A}_6^{(i)}\right| + \left|\mathrm{A}_3^{(i)}\right| \le \eta_3^{(i)} \tag{25}$$

$$\left|\left[\mathbf{w}_G^{(i)}\right]_n\right| \le \frac{1}{\sqrt{N_G^{tot}}},\ 1 \le n \le N_G^{tot}$$

To attain convexity in Equations 22 to 24, a technique using first-order approximation is essential. This is chosen to resolve the quadratic component in the beamforming vector, namely $\boldsymbol{w}_{t_1}$ from A_1A_3, $\boldsymbol{w}_{t_2}$ from A_2A_4, and $\boldsymbol{w}_G$ from A_5A_6. The approximation of a function $\left(f(x)\right)$ is stated as:

$$f\left(x^{(i)}\right) = f\left(x^{(i-1)}\right) + f'^{\left(x^{(i-1)}\right)\left(x^{(i)}-x^{(i-1)}\right)} \tag{26}$$

Therefore,

$$A_1A_3 = f\left(\boldsymbol{w}_{t_1}^{(i)}\right) = \left|\boldsymbol{h}_{V2U_1}^H\boldsymbol{w}_{t_1}^{(i)}\right|^2\left|\boldsymbol{h}_{V2U_2}^H\boldsymbol{w}_{t_1}^{(i)}\right|^2P_{V_1}^2 \tag{27}$$

the approximation of $f\left(\boldsymbol{w}_{t_1}^{(i)}\right)$ at $\boldsymbol{w}_{t_1}^{(i-1)}$ is:

$$\begin{aligned}(A_1A_3)^{approx} &= f\left(\boldsymbol{w}_{t_1}^{(i-1)}\right) + f'^{\left(w_{t_1}^{(i-1)}\right)\left(w_{t_1}^{(i)}-w_{t_1}^{(i-1)}\right)} \\ &= \left(\left(\boldsymbol{w}_{t_1}^{(i-1)H}\boldsymbol{H}_{V2U_1}\boldsymbol{w}_{t_1}^{(i-1)}\right)\left(\boldsymbol{w}_{t_1}^{(i-1)H}\boldsymbol{H}_{V2U_2}\boldsymbol{w}_{t_1}^{(i-1)}\right)P_{V_1}^2\right) + \left[\left(\left(\boldsymbol{w}_{t_1}^{(i-1)H}\boldsymbol{H}_{V2U_1}\boldsymbol{w}_{t_1}^{(i-1)}\right)\left(\boldsymbol{H}_{V2U_2}^T\boldsymbol{w}_{t_1}^{(i-1)^*}\right)\right) + \right. \\ &\quad \left.\left(\left(\boldsymbol{w}_{t_1}^{(i-1)H}\boldsymbol{H}_{V2U_2}\boldsymbol{w}_{t_1}^{(i-1)}\right)\left(\boldsymbol{H}_{V2U_1}^T\boldsymbol{w}_{t_1}^{(i-1)^*}\right)\right)P_{V_1}^2\right]^H\left(\boldsymbol{w}_{t_1}^{(i)} - \boldsymbol{w}_{t_1}^{(i-1)}\right)\end{aligned} \tag{28}$$

where,

$$\begin{aligned}f\left(\boldsymbol{w}_{t_1}^{(i-1)}\right) &= \left|\boldsymbol{h}_{V2U_1}^H\boldsymbol{w}_{t_1}^{(i-1)}\right|^2\left|\boldsymbol{h}_{V2U_2}^H\boldsymbol{w}_{t_1}^{(i-1)}\right|^2P_{V_1}^2 \\ &= \left[\left(\boldsymbol{h}_{V2U_1}^H\boldsymbol{w}_{t_1}^{(i-1)}\right)\left(\boldsymbol{w}_{t_1}^{(i-1)H}\boldsymbol{h}_{V2U_1}\right)\right]\left[\left(\boldsymbol{h}_{V2U_2}^H\boldsymbol{w}_{t_1}^{(i-1)}\right)\left(\boldsymbol{w}_{t_1}^{(i-1)H}\boldsymbol{h}_{V2U_2}\right)\right]P_{V_1}^2 \\ &= \left[\left(\boldsymbol{w}_{t_1}^{(i-1)H}\boldsymbol{h}_{V2U_1}\right)\left(\boldsymbol{h}_{V2U_1}^H\boldsymbol{w}_{t_1}^{(i-1)}\right)\right]\left[\left(\boldsymbol{w}_{t_1}^{(i-1)H}\boldsymbol{h}_{V2U_2}\right)\left(\boldsymbol{h}_{V2U_2}^H\boldsymbol{w}_{t_1}^{(i-1)}\right)\right]P_{V_1}^2 \\ &= \left[\left(\boldsymbol{w}_{t_1}^{(i-1)H}\boldsymbol{H}_{V2U_1}\boldsymbol{w}_{t_1}^{(i-1)}\right)\right]\left[\left(\boldsymbol{w}_{t_1}^{(i-1)H}\boldsymbol{H}_{V2U_2}\boldsymbol{w}_{t_1}^{(i-1)}\right)\right]P_{V_1}^2\end{aligned} \tag{29}$$

and,

$$f'\left(\boldsymbol{w}_{t_1}^{(i-1)}\right) = \left[\left(\left(\boldsymbol{w}_{t_1}^{(i-1)H}\boldsymbol{H}_{V2U_1}\boldsymbol{w}_{t_1}^{(i-1)}\right)\left(\boldsymbol{H}_{V2U_2}^T\boldsymbol{w}_{t_1}^{(i-1)^*}\right)\right) + \left(\left(\boldsymbol{w}_{t_1}^{(i-1)H}\boldsymbol{H}_{V2U_2}\boldsymbol{w}_{t_1}^{(i-1)}\right)\left(\boldsymbol{H}_{V2U_1}^T\boldsymbol{w}_{t_1}^{(i-1)^*}\right)\right)P_{V_1}^2\right]^H \tag{30}$$

Equations 29 to 32 also apply to A_2A_4 and A_5A_6, as follows:

$$A_2A_4 = f\left(\boldsymbol{w}_{t_2}^{(i)}\right) = \left|\boldsymbol{h}_{V2U_1}^H\boldsymbol{w}_{t_2}^{(i)}\right|^2\left|\boldsymbol{h}_{V2U_2}^H\boldsymbol{w}_{t_2}^{(i)}\right|^2P_{V_2}^2 \tag{31}$$

and the approximation of $f\left(\boldsymbol{w}_{t_2}^{(i)}\right)$ at $\boldsymbol{w}_{t_2}^{(i-1)}$ is:

$$\begin{aligned}(A_2A_4)^{approx} &= f\left(\boldsymbol{w}_{t_2}^{(i-1)}\right) + f'^{\left(w_{t_2}^{(i-1)}\right)\left(w_{t_2}^{(i)}-w_{t_2}^{(i-1)}\right)} \\ &= \left(\left(\boldsymbol{w}_{t_2}^{(i-1)H}\boldsymbol{H}_{V2U_1}\boldsymbol{w}_{t_2}^{(i-1)}\right)\left(\boldsymbol{w}_{t_2}^{(i-1)H}\boldsymbol{H}_{V2U_2}\boldsymbol{w}_{t_2}^{(i-1)}\right)P_{V_2}^2\right) + \left[\left(\left(\boldsymbol{w}_{t_2}^{(i-1)H}\boldsymbol{H}_{V2U_1}\boldsymbol{w}_{t_2}^{(i-1)}\right)\left(\boldsymbol{H}_{V2U_2}^T\boldsymbol{w}_{t_2}^{(i-1)^*}\right)\right) + \right. \\ &\quad \left.\left(\left(\boldsymbol{w}_{t_2}^{(i-1)H}\boldsymbol{H}_{V2U_2}\boldsymbol{w}_{t_2}^{(i-1)}\right)\left(\boldsymbol{H}_{V2U_1}^T\boldsymbol{w}_{t_2}^{(i-1)^*}\right)\right)P_{V_2}^2\right]^H\left(\boldsymbol{w}_{t_2}^{(i)} - \boldsymbol{w}_{t_2}^{(i-1)}\right)\end{aligned} \tag{32}$$

where,

$$\begin{aligned} f\left(\boldsymbol{w}_{t_2}^{(i-1)}\right) &= \left|\boldsymbol{h}_{V2U_1}^H \boldsymbol{w}_{t_2}^{(i-1)}\right|^2 \left|\boldsymbol{h}_{V2U_2}^H \boldsymbol{w}_{t_2}^{(i-1)}\right|^2 P_{V_2}^2 \\ &= \left[\left(\boldsymbol{h}_{V2U_1}^H \boldsymbol{w}_{t_2}^{(i-1)}\right)\left(\boldsymbol{w}_{t_2}^{(i-1)H} \boldsymbol{h}_{V2U_1}\right)\right]\left[\left(\boldsymbol{h}_{V2U_2}^H \boldsymbol{w}_{t_2}^{(i-1)}\right)\left(\boldsymbol{w}_{t_2}^{(i-1)H} \boldsymbol{h}_{V2U_2}\right)\right] P_{V_2}^2 \\ &= \left[\left(\boldsymbol{w}_{t_2}^{(i-1)H} \boldsymbol{h}_{V2U_1}\right)\left(\boldsymbol{h}_{V2U_1}^H \boldsymbol{w}_{t_2}^{(i-1)}\right)\right]\left[\left(\boldsymbol{w}_{t_2}^{(i-1)H} \boldsymbol{h}_{V2U_2}\right)\left(\boldsymbol{h}_{V2U_2}^H \boldsymbol{w}_{t_2}^{(i-1)}\right)\right] P_{V_2}^2 \\ &= \left[\left(\boldsymbol{w}_{t_2}^{(i-1)H} \boldsymbol{H}_{V2U_1} \boldsymbol{w}_{t_2}^{(i-1)}\right)\right]\left[\left(\boldsymbol{w}_{t_2}^{(i-1)H} \boldsymbol{H}_{V2U_2} \boldsymbol{w}_{t_2}^{(i-1)}\right)\right] P_{V_2}^2 \end{aligned} \tag{33}$$

and,

$$f'\left(\boldsymbol{w}_{t_2}^{(i-1)}\right) = \left[\left(\left(\boldsymbol{w}_{t_2}^{(i-1)H} \boldsymbol{H}_{V2U_1} \boldsymbol{w}_{t_2}^{(i-1)}\right)\left(\boldsymbol{H}_{V2U_2}^T \boldsymbol{w}_{t_2}^{(i-1)^*}\right)\right) + \left(\left(\boldsymbol{w}_{t_2}^{(i-1)H} \boldsymbol{H}_{V2U_2} \boldsymbol{w}_{t_2}^{(i-1)}\right)\left(\boldsymbol{H}_{V2U_1}^T \boldsymbol{w}_{t_2}^{(i-1)^*}\right)\right) P_{V_2}^2\right]^H \tag{34}$$

As well as for:

$$A_5 A_6 = f\left(\boldsymbol{w}_G^{(i)}\right) = \left|\boldsymbol{h}_{G2U_1}^H \boldsymbol{w}_G^{(i)}\right|^2 \left|\boldsymbol{h}_{G2U_2}^H \boldsymbol{w}_G^{(i)}\right|^2 P_G^2 \tag{35}$$

the approximation of $f\left(\boldsymbol{w}_G^{(i)}\right)$ at $\boldsymbol{w}_G^{(i-1)}$ is:

$$\begin{aligned} (A_5 A_6)^{approx} &= f\left(\boldsymbol{w}_G^{(i-1)}\right) + f'^{\left(\boldsymbol{w}_G^{(i-1)}\right)\left(\boldsymbol{w}_G^{(i)} - \boldsymbol{w}_G^{(i-1)}\right)} \\ &= \left(\left(\boldsymbol{w}_G^{(i-1)H} \boldsymbol{H}_{G2U_1} \boldsymbol{w}_G^{(i-1)}\right)\left(\boldsymbol{w}_G^{(i-1)H} \boldsymbol{H}_{G2U_2} \boldsymbol{w}_G^{(i-1)}\right) P_G^2\right) + \left[\left(\left(\boldsymbol{w}_G^{(i-1)H} \boldsymbol{H}_{G2U_1} \boldsymbol{w}_G^{(i-1)}\right)\left(\boldsymbol{H}_{G2U_2}^T \boldsymbol{w}_G^{(i-1)^*}\right)\right) + \right. \\ &\quad \left.\left(\left(\boldsymbol{w}_G^{(i-1)H} \boldsymbol{H}_{G2U_2} \boldsymbol{w}_G^{(i-1)}\right)\left(\boldsymbol{H}_{G2U_1}^T \boldsymbol{w}_G^{(i-1)^*}\right)\right) P_G^2\right]^H \left(\boldsymbol{w}_G^{(i)} - \boldsymbol{w}_G^{(i-1)}\right) \end{aligned} \tag{36}$$

where,

$$\begin{aligned} f\left(\boldsymbol{w}_G^{(i-1)}\right) &= \left|\boldsymbol{h}_{G2U_1}^H \boldsymbol{w}_G^{(i)}\right|^2 \left|\boldsymbol{h}_{G2U_2}^H \boldsymbol{w}_G^{(i)}\right|^2 P_G^2 \\ &= \left[\left(\boldsymbol{h}_{G2U_1}^H \boldsymbol{w}_G^{(i-1)}\right)\left(\boldsymbol{w}_G^{(i-1)H} \boldsymbol{h}_{G2U_1}\right)\right]\left[\left(\boldsymbol{h}_{G2U_2}^H \boldsymbol{w}_G^{(i-1)}\right)\left(\boldsymbol{w}_G^{(i-1)H} \boldsymbol{h}_{G2U_2}\right)\right] P_G^2 \\ &= \left[\left(\boldsymbol{w}_G^{(i-1)H} \boldsymbol{h}_{G2U_1}\right)\left(\boldsymbol{h}_{G2U_1}^H \boldsymbol{w}_G^{(i-1)}\right)\right]\left[\left(\boldsymbol{w}_G^{(i-1)H} \boldsymbol{h}_{G2U_2}\right)\left(\boldsymbol{h}_{G2U_2}^H \boldsymbol{w}_G^{(i-1)}\right)\right] P_G^2 \\ &= \left[\left(\boldsymbol{w}_G^{(i-1)H} \boldsymbol{H}_{G2U_1} \boldsymbol{w}_G^{(i-1)}\right)\right]\left[\left(\boldsymbol{w}_G^{(i-1)H} \boldsymbol{H}_{G2U_2} \boldsymbol{w}_G^{(i-1)}\right)\right] P_G^2 \end{aligned} \tag{37}$$

$$f'\left(\boldsymbol{w}_G^{(i-1)}\right) = \left[\left(\left(\boldsymbol{w}_G^{(i-1)H} \boldsymbol{H}_{G2U_1} \boldsymbol{w}_G^{(i-1)}\right)\left(\boldsymbol{H}_{G2U_2}^T \boldsymbol{w}_G^{(i-1)^*}\right)\right) + \left(\left(\boldsymbol{w}_G^{(i-1)H} \boldsymbol{H}_{G2U_2} \boldsymbol{w}_G^{(i-1)}\right)\left(\boldsymbol{H}_{G2U_1}^T \boldsymbol{w}_G^{(i-1)^*}\right)\right) P_G^2\right]^H \tag{38}$$

The approximation results of Equations 28, 32, and 36 are substituted into Equations 23 to 25, respectively, replacing $A_1 A_3$, $A_2 A_4$, and $A_5 A_6$. Ultimately, the optimization of the beamforming vector can be solved by the AIS algorithm with a first-order approximation approach, where the magnitude operator |.| in the objective function of Problems 22-25 is a real number. The factors $\eta_1^{(i)}$, $\eta_2^{(i)}$, and $\eta_3^{(i)}$ are interference suppression factors whose values are obtained from the expression $\eta_j^{(i)} = \eta + \mu_j^{(i)}$ for $j = \{1,2,3\}$. These factors are used to reduce interference from the SI and G2U channels. η is a non-negative lower bound for the interference suppression factor, defined as: $\eta = min\left\{\frac{\sigma_V^2}{10\sqrt{P_S}}, \frac{\sigma_{U_k}^2}{10\sqrt{P_V}}\right\}$. Meanwhile, the values of $\mu_j^{(i)}$ are determined as described in Algorithm 1, step 16, and are influenced by κ, which is the step size used for self-interference suppression adjustment. The process will stop when the rate increases fall below the convergence threshold of $\boldsymbol{\epsilon}_r = 0.01$ bps/Hz. The optimal beamforming vector will then be normalized to meet the CM constraints.

Power optimization is the final suboptimal step to maximize the achievable rate further. This step must consider power transferred to prevent unnecessary power loss. The optimal power allocation for the gateway and UAV is performed through an iterative process to achieve an achievable rate on the G2V≈V2U links. If $P_G^\star$ represents the optimal transmit power of the gateway, and $P_{V_k}^\star$ represents the transmit power of the UAV to each UE, both are assumed to be less than the maximum transmit power and must be non-negative, satisfying $0 < P_G^\star < P_G$, $0 < P_V^\star < P_V$, $P_V^\star = \sum P_{V_k}^\star$, and $P_{V_k}^\star > 0$.

Algorithm 1. Iterative Algorithm to Jointly Optimize Positioning, Beamforming, and Power Allocation for Millimeter Wave Full Duplex UAV System

1. Initialize UAV location x^o, y^o, and h^o, then calculate (x^o, y^o, h^o).
2. **if** (x^o, y^o, h^o) is already in LOS condition, then
3. set $(x^\star, y^\star, h^\star) = (x^o, y^o, h^o)$.
4. **else**
5. Initiate $t = 0$.
6. Update $t = t + 1$, terminate when LOS conditions for G2V and V2U are found.
7. Determine $(x^\star, y^\star, h^\star)$ based on LOS conditions and the shortest distance from the initial position.
8. **end if**
9. Estimate channel matrices $\boldsymbol{H}_{G2V}$, $\boldsymbol{H}_{SI}$, $\boldsymbol{h}_{V2U1}$, $\boldsymbol{h}_{V2U2}$, and $\boldsymbol{h}_{G2U}$.
10. Initialize $i = 0$.
11. Initialize $\boldsymbol{w}_G^{(0)}$, $\boldsymbol{w}_r^{(0)}$, and $\boldsymbol{w}_{t_k}^{(0)}$ according to (19).
12. Initialize $\mu_2^{(0)} = \left|\boldsymbol{w}_r^{(0)H} \boldsymbol{H}_{SI} \boldsymbol{w}_{t_k}^{(0)}\right|$.
13. Calculate $R_{G2U}^{(0)}$ according to (12) and define $R_{G2U}^{(-1)} = -\infty$.
14. **while** $R_{G2U}^{(i)} - R_{G2U}^{(i-1)} > \epsilon_r$ **do**
15. $i = i + 1$.
16. Update the suppression factor $\mu_j^{(i)} = \frac{\mu_{j+1}^{(i-1)}}{\kappa}$ for $j = 1, 3$, $\mu_j^{(i)} = \frac{\mu_{j-1}^{(i)}}{\kappa}$ for $j = 2$, and $\eta_j^{(i)} = \eta + \mu_j^{(i)}$ for $j = 1, 2, 3$.
17. Solve (22) to obtain $\boldsymbol{w}_r^o$.
18. Normalize $\boldsymbol{w}_r^o$ to satisfy the CM constraint and obtain $\boldsymbol{w}_r^{(i)}$.
19. Solve (23) and (24) to obtain $\boldsymbol{w}_{t_k}^o$.
20. Normalize $\boldsymbol{w}_{t_k}^o$ to satisfy the CM constraint and obtain $\boldsymbol{w}_{t_k}^{(i)}$.
21. Solve (25) to obtain $\boldsymbol{w}_G^o$.
22. Normalize $\boldsymbol{w}_G^o$ to satisfy the CM constraint and obtain $\boldsymbol{w}_G^{(i)}$.
23. Obtain $P_G^{(i)}$ and $P_{V_k}^{(i)}$.
24. Calculate $R_{G2U}^{(i)}$ according to (12).
25. **end while**
26. $\boldsymbol{w}_r^\star = \boldsymbol{w}_r^{(i)}$, $\boldsymbol{w}_{t_k}^\star = \boldsymbol{w}_{t_k}^{(i)}$, $\boldsymbol{w}_G^\star = \boldsymbol{w}_G^{(i)}$, $P_G^\star = P_G^{(i)}$, and $P_{V_k}^\star = P_{V_k}^{(i)}$
27. **return** $x^\star, y^\star, h^\star, \boldsymbol{w}_G^\star, \boldsymbol{w}_r^\star, \boldsymbol{w}_{t_k}^\star, P_G^\star, P_{V_k}^\star$

To maximize the achievable rate, if the rate on the G2V link is lower than the V2U link, the UAV's transmit power should be reduced, and vice versa. This approach prevents power wastage. Additionally, the G2V link rate is generally assumed to be the bottleneck (much lower than the V2U link rate). Algorithm 1 summarizes of the position, beamforming, and power allocation optimization solutions for the UAV systems.

Algorithm 1 draws inspiration from the work by Zhu et al. [34], yet it displays numerous distinctions. During the initial step, the algorithm does not rely on Theorem 1 to determine the optimal position; instead, it utilizes mathematical calculations to ascertain the midpoint. Channel estimation is conducted for both matrix and vector channels in the ninth step. The optimization of vector beamforming achieves interference reduction through a first-order approximation approach. Significant differences exist between the first-order approximation approach of the beamforming vector and the power optimization iteration process, resulting in substantial divergence.

4- Results and Discussion

This results section presents the performance evaluation of the proposed optimization formula and verifies the maximum achievable rate. It also compares the proposed scheme with other existing schemes, single UE and multi-UE, for the different sizes of UPA antenna and optimum power transmission for the different UPA sizes. Validation is performed through simulation with the primary parameters tabulated in Table 1.

Table 1. Simulation parameters

Notation	Definition	Value
ϵ_r	The threshold value for convergence	0.05 bps/Hz
κ	Step size parameter to reduce suppression factor	10
σ_V^2 and $\sigma_{U_k}^2$	The noise power at UAV and UE_k	–110 dBm
χ_{Link}^{LOS}	Random variable for LOS path	1
χ_{Link}^{NLOS}	Random variable for NLOS path	0
a	Positive modelling parameters that determine the probability of existing LOS path	11.95
b	Positive modelling parameters that determine the probability of existing LOS path	0.14
f	Carrier frequency	38 GHz
h_{min}	The minimum altitude of the UAV	100 m
h_{max}	The maximum altitude of the UAV	300 m
i	Iteration	10
L	Number of NLOS components	4
$M_\tau \times N_\tau$	Antenna array size	4×4
P_G and P_V	The maximum transmits power of Gateway and UAV	20 dBm
P_{V_k}	The UAV transmits power to the k^{th} UE (initialization)	P_V/K
$r_{m,n}$	The distance between the m^{th} transmitter array element and the n^{th} receiver array element	10λ
S	Gateway coordinate	(0,0,0)
x and y	The maximum postion of the UAV on *x*-axis and *y*-axis	200 m

In determining the optimal location for UAV, each UE is allocated an equal share of the total transmitted power. This allocation assumes that all antennas are isotropic and independent of each other. The system operates under ideal conditions with pure LOS, meaning there are no obstacles obstructing direct transmission paths, and it assumes an ideal beamforming scenario where signals are precisely directed towards their intended recipients.

The gateway is positioned at the coordinates (0,0,0), while the UE locations are randomly distributed. The UAV's position along the *x*-axis and *y*-axis is determined through mathematical calculations. Once these coordinates are established, the UAV is assigned a minimum altitude of 100 meters, resulting in an initial position of $V(70,60,100)$. Despite this, the UAV can still enhance the probability of maintaining a LOS link. To achieve this, the UAV moves around its initial position (V) to identify the point with the highest LOS probability, eventually finding it at $V^o(80,70,110)$. However, this new position involves a significant movement from the starting point, which does not meet the requirements for minimal displacement. Therefore, a position with a shorter distance is selected. Ultimately, the UAV's optimal position, which maximizes the LOS path probability while minimizing displacement, is determined to be $V^\star(80,61,110)$.

After determining the optimal position for the UAV, the next step involves implementing vector beamforming and power optimization to achieve the highest possible data transmission rate. Figure 3 demonstrate the effectiveness of the proposed joint optimization approach for UAV-enabled communication systems. Specifically, the method that simultaneously optimizes the UAV's position, beamforming vectors, and transmit power achieves the highest data rate, converging to approximately 6.25 bps/Hz within just four iterations. This rapid convergence highlights the efficiency of the proposed algorithm. In contrast, methods that exclude one or more optimization components show significantly reduced performance. For instance, the approach without power optimization achieves a lower but steady rate of about 2.1 bps/Hz, indicating that power control plays a critical role in enhancing communication efficiency. Similarly, optimizing only the beamforming vectors while keeping the UAV position and power fixed yields a comparable but slightly lower rate. The scenario without any optimization performs the worst, with the rate remaining near zero throughout the iterations. These findings underscore the importance of integrating all three components—positioning, beamforming, and power allocation—for maximizing the transmission rate in UAV-assisted networks.

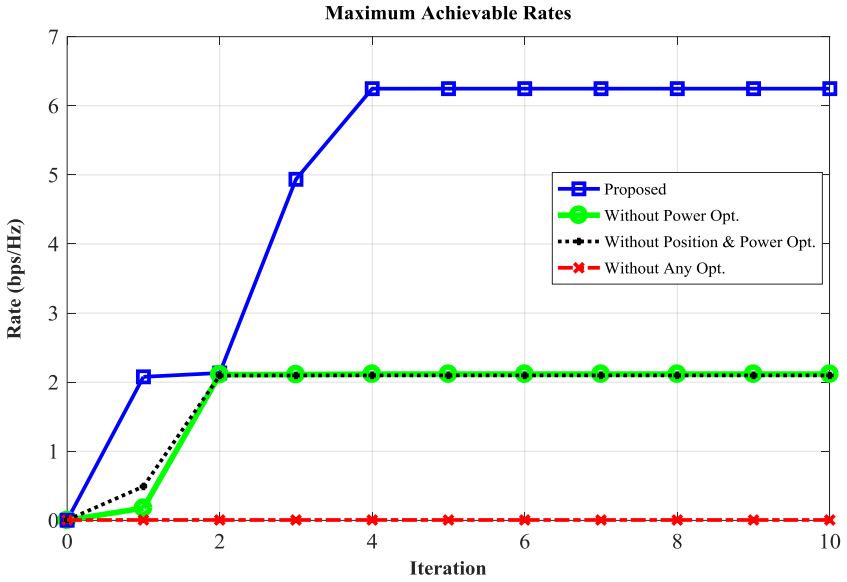

Figure 3. Superior of proposed scheme

The simulation results present the proposed achievable rate for two UEs and compare it to the findings in Zhu et al. [34], which only consider a single UE, as illustrated in Figure 4. As shown in the figure, the achievable rate of the proposed method stabilizes around 6.25 bps/Hz, whereas the reference method reaches a significantly higher rate of approximately 13.8 bps/Hz. This performance gap is attributed to the presence of inter-user interference in the two-UE scenario, which is absent in the single-UE setting of Zhu et al. [34]. Despite the lower rate, the proposed system demonstrates achieving near-optimal performance by the second iteration. This efficiency is primarily due to the implementation of an interference suppression mechanism that effectively mitigates both inter-user interference and SI. Consequently, while the overall rate is reduced due to the more complex communication environment, the system's ability to quickly stabilize underscores the effectiveness of the proposed optimization framework in managing interference in multi-user UAV-enabled networks.

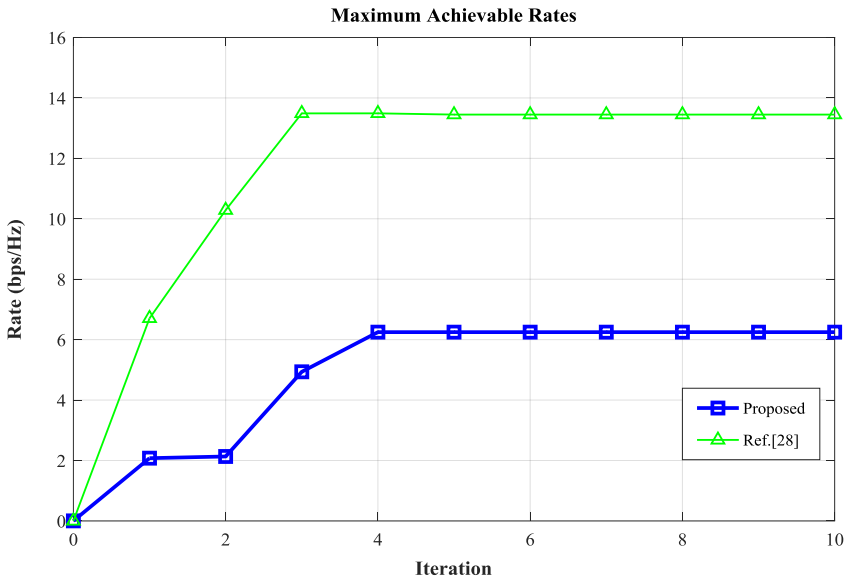

Figure 4. Multiple UE approximation

The transmit power optimization ultimately yields the maximum rate. The beamforming optimization leads to a significantly higher achievable rate on the G2V link compared to the V2U link, necessitating a reduction in the transmit power on the gateway (P_G). Meanwhile, the UAV's transmitted power (P_V) is maintained close to its maximum permissible value. Figure 5 illustrates the convergence behavior of the optimal power allocation at both the gateway ($P_G^\star$) and the UAV ($P_V^\star$) across multiple iterations of the optimization algorithm. Initially, both $P_G^\star$ and $P_V^\star$ start at relatively high values, with the UAV's power nearly at its maximum permissible level and the gateway power also elevated. However, as the optimization progresses, $P_G^\star$ is significantly reduced, ultimately converging to a minimal value near 0 dBm by the fourth iteration. In contrast, $P_V^\star$ stabilizes close to 18.5 dBm, indicating that the UAV maintains a high transmit power throughout.

This behavior aligns with the beamforming optimization, the power on G2V (Gateway-to-Vehicle) link becomes substantially more efficient than the V2U (Vehicle-to-UAV) link. To mitigate excessive interference and maintain balanced rate performance, the system compensates by minimizing gateway transmit power, thereby preserving the integrity of the V2U link. The result showcases the adaptability of the proposed method in dynamically reallocating power to achieve an optimal trade-off between links, even in scenarios with only two UEs, where interlink interference still plays a critical role. Compared to previous work that may have assumed less significant interference in low-UE-count systems, this outcome highlights the importance of joint optimization in multi-link environments. Significantly higher achievable rate on the G2V link compared to the V2U link, necessitating a reduction in P_G. Meanwhile, P_V is maintained close to its maximum permissible value. Figure 5 shows the optimal power allocation on the gateway $(P_G^\star)$ and UAV $(P_V^\star)$.

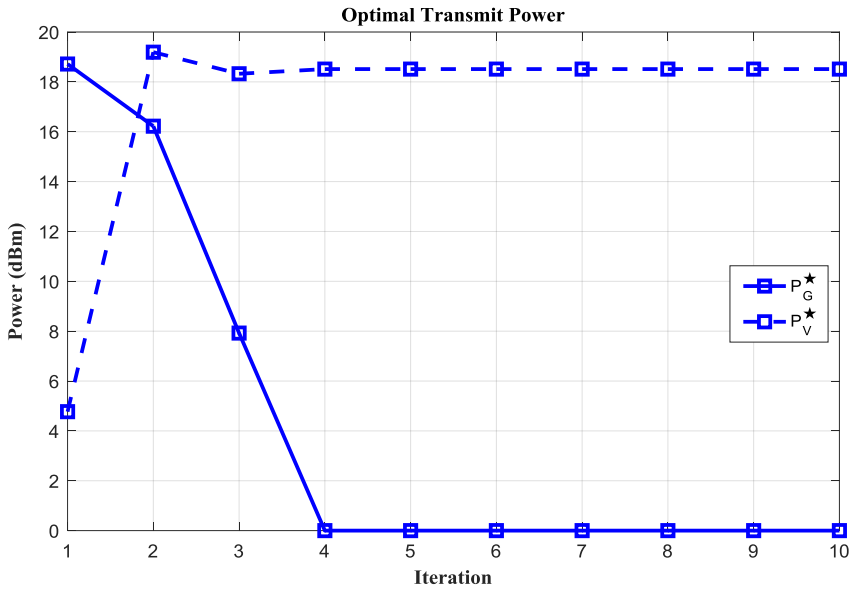

Figure 5. Optimal transmits power allocation of G2V and V2U links of the proposed scheme with 10 iterations

Figure 6 further substantiates the direct relationship between transmitted power and achievable rate by illustrating the convergence behavior of the rate over iterative computations for three different power levels: 10 dBm, 20 dBm, and 30 dBm. As depicted in the figure, the achievable rate increases with each iteration until it stabilizes, with higher transmit power levels converging to higher rate values. Specifically, when the transmit power is set to 10 dBm, the rate converges to approximately 6.2 bps/Hz, while at 20 dBm and 30 dBm, the rate reaches around 6.3 bps/Hz and 10 bps/Hz, respectively. This demonstrates that with grea0 ter transmit power, the system benefits from a higher SINR, enabling a more efficient and robust data transmission.

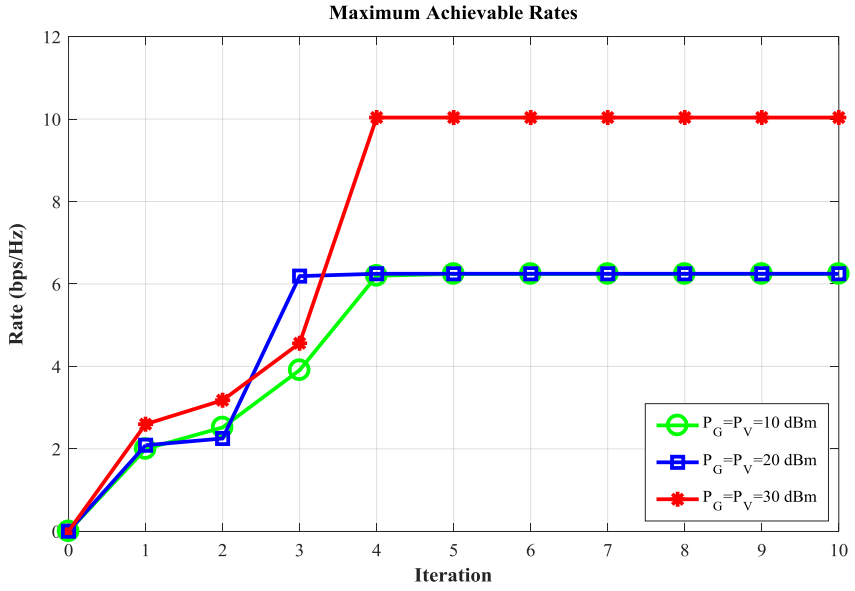

Figure 6. Maximum achievable rate for a G2U link with 10 iterations under varying the maximum transmit power

Figure 7 offers a detailed view of the optimal power allocation dynamics for both the gateway (P_G) and the UAV (P_V) under varying initial maximum transmit power settings: 10 dBm, 20 dBm, and 30 dBm. The two subplots illustrate how the optimization algorithm converges across iterations for each scenario, prioritizing power efficiency while ensuring rate performance. Figure 7(a) shows the gateway's power (P_G) undergoes a substantial reduction across iterations, regardless of the initial power level. Notably, even when starting from a high transmit power of 30 dBm, the gateway power is gradually reduced to nearly 0 dBm by the fourth iteration. This behavior highlights the core objective of the optimization strategy: to minimize unnecessary power usage, particularly at the gateway, which introduces significant SI if operated at high power. The rapid convergence to low gateway power levels across all initial conditions supports the effectiveness of the interference-aware design. Figure 7(b) shows the tracking of the UAV's power (P_V), which behaves differently. Instead of being reduced, P_V is retained at relatively high levels, particularly when higher transmit power budgets are available. For example, in the 30 dBm case, the UAV's power stabilizes near the upper limit after just three iterations. This aligns with the system design philosophy: the UAV, benefiting from beamforming and reduced interference, is allowed to transmit at higher power to maximize the end-to-end data rate, while the gateway dynamically adjusts its power based on feedback and interference levels.

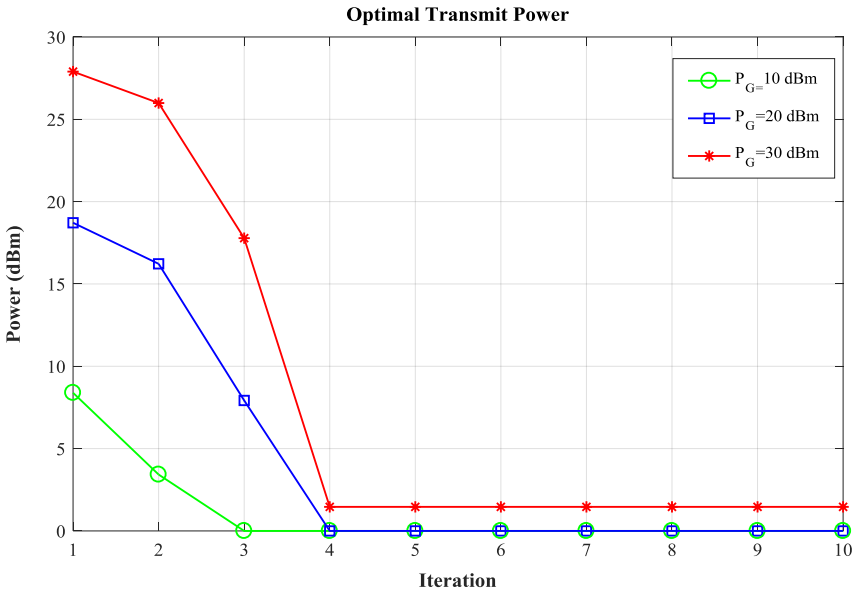

(a)

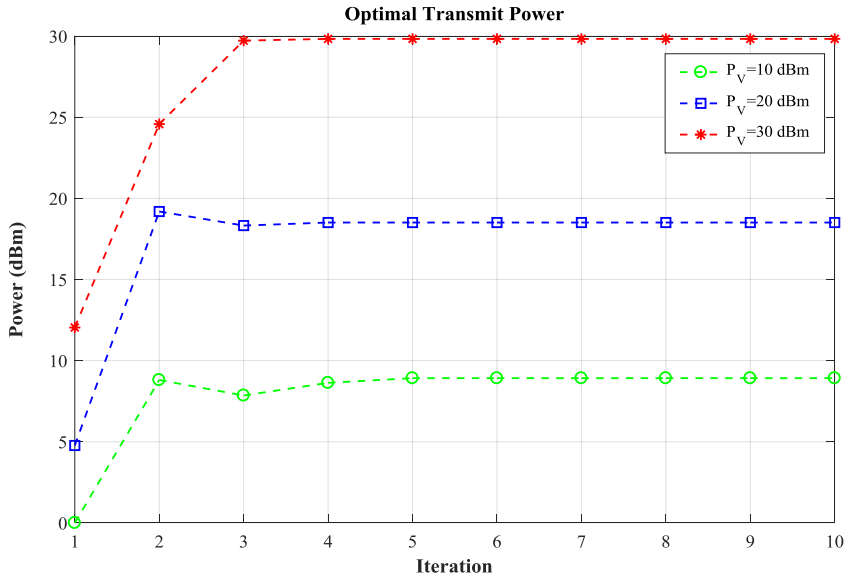

(b)

Figure 7. Optimal power transmit allocation with 10 iterations under varying the maximum transmit power: (a) G2V link and (b) V2U link

It emphasises a cooperative power control strategy. The UAV provides feedback on achievable rate, enabling the gateway to tailor its transmit power precisely, thus achieving rate goals without power wastage. This method outperforms static high-power transmission approaches by limiting SI, and optimizing computation and energy efficiency, especially critical in scenarios involving UAV-based communication relays.

A thorough comparison of our suggested framework with a number of illustrative works in the field of UAV-assisted wireless communication is given in Table 2. In addition to their obtained results, these studies are assessed according to the types of communication links they take into account, how they handle non-convex optimization, and whether they incorporate position, beamforming, and power optimization. Early studies like Yang et al. [20] and Xu et al. [26] mostly concentrated on improving uplink or downlink performance by jointly optimizing UAV parameters like power, location, and altitude. They did not, however, specifically address the underlying optimization problems' non-convexity. Similar advancements were made by Niu et al. [25] and Abbasi & Yanikomeroglu [29], who took into account bandwidth and SINR optimization, respectively; however, non-convexity was only partially or indirectly addressed by their approaches. Full-Duplex (FD) UAV systems with beamforming and positioning have been studied recently, with efforts like Zhu et al. [34] providing better rate performance. However, these studies typically focus on a single user scenario and still fail to fully address beamforming complexity, particularly when it comes to mmWave communication, and do not fully incorporate all important optimization components at the same time. On the other hand, this paper presents a new joint optimization framework that takes into account both access (downlink) and backhaul (uplink) links for a multi-user mmWave FD UAV relay system. First-order approximation and iterative decomposition into subproblems are used to explicitly address the problem's inherent non-convexity, ensuring tractable and convergent solution pathways. Furthermore, in contrast to earlier studies, this study combines power and position optimization with hybrid beamforming optimization, which is essential for realistic mmWave hardware implementation. In a multi-user FD environment, the suggested approach shows noticeably higher achievable rates while preserving power efficiency and user equity. This work stands out from previous literature due to its thorough design and optimization features, which make it a reliable and scalable solution for UAV communication systems of the future.

Table 2. Comparison of the proposed method with previous studies

Reference	Method	Communication Link	Non-Convex Handling	Position Optimization	Beamforming Optimization	Power Optimization	Outcome
Yang et al. [20]	Joint optimization of UAV altitude, beamwidth, location, power	Uplink	Not explicitly addressed	✔	✘	✔	Minimize total uplink power with QoS constraints
Niu et al. [25]	Joint 3D position, power, bandwidth	Downlink	Considered statistical QoS	✔	✘	✔	Maximize effective capacity
Xu et al. [26]	Location, transmit power, bandwidth allocation	Uplink & Downlink	Not explicitly addressed	✔	✘	✔	Minimize transmission delay
Abbasi & Yanikomeroglu [29]	Optimization for max-min SINR	Uplink & Downlink	Partial	✔	✘	✔	Maximize user SINR
Zhu et al. [34]	FD UAV system with beamforming and positioning	Uplink & Downlink	Partial, single-user	✔	✔	✔	Achievable rate maximized (single-user)
Present Study	Joint optimization using first-order approximation and iterative decomposition into subproblems	Uplink (Backhaul) + Downlink (Access) in mmWave FD UAV	Explicitly addressed via first-order approximation and subproblem decomposition	✔	✔ (Hybrid beamforming)	✔	Significantly improved achievable rate in multi-user FD UAV relay system; power-efficient and fair

5- Conclusion

This study focuses on enhancing communication capabilities in mmWave networks using a full-duplex UAV relay to achieve maximum data rates for UE. By optimizing the UAV position, beamforming vectors, and power allocation, a new algorithm for multiple UE scenarios was developed to increase achievable rates significantly. The proposed algorithm was validated through MATLAB simulations, showing improved performance compared to solutions without optimization. The research emphasizes the importance of joint optimization in maximizing achievable rates and minimizing power wastage in UAV communication systems. Furthermore, the study introduces an iterative solution for multi-UE scenarios and a first-order approximation approach, effectively addressing complex problems and optimizing data transmission rates. Optimization involves determining the optimal UAV position, designing beamforming vectors, and allocating transmit power to enhance the end-to-end achievable rate. Simulation results demonstrate the effectiveness of the proposed optimization formula compared to existing schemes, showcasing superior performance through integrated optimization of UAV position, beamforming vectors, and power allocation. Overall, the research presents a novel approach to maximizing data rates in UAV communication systems through comprehensive optimization strategies, paving the way for efficient and power-saving transmission in future wireless communication scenarios.

However, in simulations, especially for power optimization, because the iterations are quite long, a simulation device with higher specifications is required so that the power increase step size can be smaller. Important to highlight, while the proposed algorithm is effective, its computational complexity may limit scalability and runtime efficiency on lower-performance hardware. Future work should focus on reducing this overhead through methods like dimensionality reduction, heuristic initialization, or parallel processing to improve real-time applicability. Moreover, enhancing the algorithm’s adaptability to dynamic conditions such as UE mobility and channel fading will increase its practicality. With these improvements, the framework could serve as a strong foundation for intelligent UAV-based systems in next-generation wireless networks.

6- Declarations

6-1- Author Contributions

Conceptualization, D.H., I.Z., and I.; methodology, D.H. and I.Z.; software, D.H.; validation, D.H., I.Z., and I.; formal analysis, D.H.; investigation, D.H.; resources, D.H.; data curation, D.H.; writing—original draft preparation, D.H.; writing—review and editing, D.H., I.Z. and I.; visualization, D.H.; supervision, I.Z. and I.; project administration, D.H.; funding acquisition, D.H., I.Z., and I. All authors have read and agreed to the published version of the manuscript.

6-2- Data Availability Statement

The data presented in this study are available on request from the corresponding author.

6-3- Funding

The work of Irma Zakia and Dwi Harinitha was partially supported by the Indonesian Ministry of Education, Culture, Research, and Technology under the 2023 Postgraduate Scheme (PPS), Doctoral Program. The work of Iskandar was partially supported by the National Research and Innovation Agency (BRIN), Indonesia.

6-4- Institutional Review Board Statement

Not applicable.

6-5- Informed Consent Statement

Not applicable.

6-6- Conflicts of Interest

The authors declare that there is no conflict of interest regarding the publication of this manuscript. In addition, the ethical issues, including plagiarism, informed consent, misconduct, data fabrication and/or falsification, double publication and/or submission, and redundancies have been completely observed by the authors.

7- References

[1] Yu, X., Huang, X., Wang, K., Shu, F., & Dang, X. (2022). Joint Design of Power Allocation, Beamforming, and Positioning for Energy-Efficient UAV-Aided Multiuser Millimeter-Wave Systems. IEEE Journal on Selected Areas in Communications, 40(10), 2930–2945. doi:10.1109/JSAC.2022.3196111.

[2] Wang, X., Kong, L., Kong, F., Qiu, F., Xia, M., Arnon, S., & Chen, G. (2018). Millimeter wave communication: A comprehensive survey. IEEE Communications Surveys and Tutorials, 20(3), 1616–1653. doi:10.1109/COMST.2018.2844322.

[3] Heimann, K., Häger, S., & Wietfeld, C. (2022). 5.5 Potential of Millimeter Wave Communications. Applications, 375–390, De Gruyter Brill, Berlin, Germany. doi:10.1515/9783110785982-029.

[4] Kong, H., Huang, C., Yu, J., & Shen, X. (2025). A Survey of mmWave Radar-Based Sensing in Autonomous Vehicles, Smart Homes and Industry. IEEE Communications Surveys & Tutorials, 27(1), 463–508. doi:10.1109/comst.2024.3409556.

[5] Randles, H., Newcombe, A., Taberner, A., Budgett, D., & Nielsen, P. (2023). Optimising Multi-Wavelength Attenuation-Based Length Sensors. IEEE International Instrumentation and Measurement Technology Conference (I2MTC-2023), 1–6. doi:10.1109/i2mtc53148.2023.10175970.

[6] Ruiz, C. G., Pascual-Iserte, A., & Munoz, O. (2021). Analysis of Blocking in mmWave Cellular Systems: Application to Relay Positioning. IEEE Transactions on Communications, 69(2), 1329–1342. doi:10.1109/TCOMM.2020.3038177.

[7] An, H. T., Ren, J. F., Huo, J. C., He, Y., & Xu, L. (2022). Short-distance Attenuation of Electromagnetic Waves in Rainfall Environment. 2022 IEEE MTT-S International Microwave Workshop Series on Advanced Materials and Processes for RF and THz Applications (IMWS-AMP), 1–3. doi:10.1109/imws-amp54652.2022.10107021.

[8] Gupta, A. K., Andrews, J. G., & Heath, R. W. (2018). Macrodiversity in Cellular Networks with Random Blockages. IEEE Transactions on Wireless Communications, 17(2), 996–1010. doi:10.1109/TWC.2017.2773058.

[9] Sur, S., & Nelakuditi, S. (2022). A Case for Line-Of-Sight Blockage Detection as a Primitive in Millimeter-Wave Networks. Proceedings - 2022 IEEE 19th International Conference on Mobile Ad Hoc and Smart Systems, MASS 2022, 564–569. doi:10.1109/MASS56207.2022.00084.

[10] Hersyandika, R., Sanchez, J., Miao, Y., Pollin, S., & Tufvesson, F. (2022). Measurement-based blockage and intra-cluster interference analysis in mmWave multi-point connectivity networks. EmergingWireless 2022 - Proceedings of the 1st International Workshop on Emerging Topics in Wireless, Part of CoNEXT 2022, 12–17. doi:10.1145/3565474.3569071.

[11] Zhang, Y., & Mishra, D. (2024). Energy-Efficient UAV-Relayed High-altitude Platform to Ground User Communication. IEEE International Symposium on Personal, Indoor and Mobile Radio Communications, PIMRC, 1–6. doi:10.1109/PIMRC59610.2024.10817374.

[12] Tran, G. K. (2024). Temporary Communication Network Using Millimeter-Wave Drone Base Stations. 2024 IEEE VTS Asia Pacific Wireless Communications Symposium, APWCS 2024, 1–5. doi:10.1109/APWCS61586.2024.10679283.

[13] Zhang, C., Zhang, L., Zhu, L., Zhang, T., Xiao, Z., & Xia, X. G. (2021). 3D Deployment of Multiple UAV-Mounted Base Stations for UAV Communications. IEEE Transactions on Communications, 69(4), 2473-2488. doi:10.1109/TCOMM.2021.3049387.

[14] Chen, K., Wang, Y., Zhao, J., Wang, X., & Fei, Z. (2021). URLLC-Oriented Joint Power Control and Resource Allocation in UAV-Assisted Networks. IEEE Internet of Things Journal, 8(12), 10103–10116. doi:10.1109/JIOT.2021.3051322.

[15] Yu, B., Qian, C., Lin, P., Shao, S., Pan, W., Shen, Y., Hu, S., Su, D., Sun, C., Xiong, Q., & Lee, J. (2022). Full Duplex Communication with Practical Self-Interference Cancellation Implementation. ICC 2022 - IEEE International Conference on Communications, 1100–1105. doi:10.1109/icc45855.2022.9838784.

[16] Sultan, R., Seddik, K., Han, Z., & Aazhang, B. (2021). Joint Transmitter-Receiver Optimization and Self-Interference Suppression in Full-Duplex MIMO Systems. IEEE Transactions on Vehicular Technology, 70(7), 6913–6929. doi:10.1109/TVT.2021.3087181.

[17] Ali, S., Ghazanfari, A., Rajatheva, N., & Latva-Aho, M. (2014). Effect of Residual of Self-Interference in Performance of Full-Duplex D2D Communication. Proceedings of the 1st International Conference on 5G for Ubiquitous Connectivity, 46-51. doi:10.4108/icst.5gu.2014.258100.

[18] Zhang, Y., Xiao, M., Han, S., Skoglund, M., & Meng, W. (2019). On Precoding and Energy Efficiency of Full-Duplex Millimeter-Wave Relays. IEEE Transactions on Wireless Communications, 18(3), 1943–1956. doi:10.1109/twc.2019.2900038.

[19] Zhang, J., Garg, N., Holm, M., & Ratnarajah, T. (2021). Design of Full Duplex Millimeter-Wave Integrated Access and Backhaul Networks. IEEE Wireless Communications, 28(1), 60–67. doi:10.1109/MWC.001.2000199.

[20] Yang, Z., Pan, C., Shikh-Bahaei, M., Xu, W., Chen, M., Elkashlan, M., & Nallanathan, A. (2018). Joint Altitude, Beamwidth, Location, and Bandwidth Optimization for UAV-Enabled Communications. IEEE Communications Letters, 22(8), 1716–1719. doi:10.1109/LCOMM.2018.2846241.

[21] Andreou, A., Mavromoustakis, C. X., Batalla, J. M., Markakis, E., Bourdena, A., Mastorakis, G., & Song, H. (2024). Enhancing UAV Network Efficiency through 6G+ Enabled Federated Learning Algorithms and Energy optimization Techniques. 2024 International Wireless Communications and Mobile Computing (IWCMC), 192–197. doi:10.1109/iwcmc61514.2024.10592391.

[22] Yang, Z., Pan, C., Wang, K., & Shikh-Bahaei, M. (2019). Energy Efficient Resource Allocation in UAV-Enabled Mobile Edge Computing Networks. IEEE Transactions on Wireless Communications, 18(9), 4576–4589. doi:10.1109/TWC.2019.2927313.

[23] Shuai, J., He, Y., Cao, X., & Xie, L. (2024). Energy Consumption Minimization for UAV-Mounted Active RIS-Assisted Mobile Edge Computing. 2024 IEEE International Workshop on Radio Frequency and Antenna Technologies (IWRF & AT), 516–521. doi:10.1109/iwrfat61200.2024.10594363.

[24] Wang, Z., Wang, G., & Huang, S. (2024). Energy-efficient mobile edge computing assisted by layered UAVs based on convex optimization. Physical Communication, 65, 62062007. doi:10.1016/j.phycom.2024.102382.

[25] Niu, H., Zhao, X., & Li, J. (2021). 3D Location and Resource Allocation Optimization for UAV-Enabled Emergency Networks under Statistical QoS Constraint. IEEE Access, 9, 41566–41576. doi:10.1109/ACCESS.2021.3065055.

[26] Xu, L., Chen, M., Chen, M., Yang, Z., Chaccour, C., Saad, W., & Hong, C. S. (2021). Joint Location, Bandwidth and Power Optimization for THz-Enabled UAV Communications. IEEE Communications Letters, 25(6), 1984–1988. doi:10.1109/LCOMM.2021.3064067.

[27] Wang, F., Zhang, Z., Zhou, L., Shang, T., & Zhang, R. (2024). Robust Multi-UAV Cooperative Trajectory Planning and Power Control for Reliable Communication in the Presence of Uncertain Jammers. Drones, 8(10), 558. doi:10.3390/drones8100558.

[28] Solati, A., Moghaddam, J. Z., & Ardebilipour, M. (2024). Enhancing Disaster Communication: Multi-UAV Optimization for Efficient Coverage. 2024 32nd International Conference on Electrical Engineering (ICEE), 1–5. doi:10.1109/icee63041.2024.10668219.

[29] Abbasi, O., & Yanikomeroglu, H. (2024). UxNB-Enabled Cell-Free Massive MIMO With HAPS-Assisted Sub-THz Backhauling. IEEE Transactions on Vehicular Technology, 73(5), 6937–6953. doi:10.1109/TVT.2023.3347140.

[30] Hassan, H., Althunibat, S., Dabiri, M. T., Hasna, M., & Qaraqe, K. (2024). On the Error Analysis of Two-Way Relaying in mmWave-Based Aerial Links. IEEE Wireless Communications and Networking Conference, WCNC, 1–6. doi:10.1109/WCNC57260.2024.10570604.

[31] Harinitha, D., Zakia, I., Iskandar, & Kurniawan, A. (2022). Effect of Different Locations of Millimeter Wave HAPS on the Downlink Sum Rate. 2022 16th International Conference on Telecommunication Systems, Services, and Applications (TSSA), 1–5. doi:10.1109/tssa56819.2022.10063916.

[32] Liu, W., Zhang, X., Xing, H., Ren, J., Shen, Y., & Cui, S. (2025). UAV-Enabled Wireless Networks With Movable-Antenna Array: Flexible Beamforming and Trajectory Design. IEEE Wireless Communications Letters, 14(3), 566–570. doi:10.1109/LWC.2024.3451246.

[33] Hashir, S. M., Gupta, S., Megson, G., Aryafar, E., & Camp, J. (2022). Rate Maximization in a UAV Based Full-Duplex Multi-User Communication Network Using Multi-Objective Optimization. Electronics, 11(3), 401. doi:10.3390/electronics11030401.

[34] Zhu, L., Zhang, J., Xiao, Z., Cao, X., Xia, X. G., & Schober, R. (2020). Millimeter-Wave Full-Duplex UAV Relay: Joint Positioning, Beamforming, and Power Control. IEEE Journal on Selected Areas in Communications, 38(9), 2057–2073. doi:10.1109/JSAC.2020.3000879.

[35] Li, Y., Pan, W., Jiwu, G., Shi, C., Hu, N., & Shao, S. (2024). Millimeter-Wave Full-Duplex Phased Array RF Self-Interference Cancellation Technology. 2024 IEEE International Conference on Communications Workshops, ICC Workshops 2024, 1091–1096. doi:10.1109/ICCWorkshops59551.2024.10615922.

[36] Nguyen, B. C., Hoang, T. M., Dung, L. T., Kim, T., & Vinh, N. Van. (2022). On performance of full-duplex UAV system with multiple NOMA users and millimeter-wave communications. Physical Communication, 55. doi:10.1016/j.phycom.2022.101895.

[37] Ding, Q., Luo, Y., Yang, R., Hu, J., & Luo, C. (2022). Joint deployment, beamforming and power allocation of MmWave full-duplex UAV-BS. Proceedings of the 5th International ACM Mobicom Workshop on Drone Assisted Wireless Communications for 5G and Beyond, 127–132. doi:10.1145/3555661.3560876.

[38] Mahmood, M., Yuan, Y., & Le-Ngoc, T. (2024). Multiple UAV-Assisted Cooperative DF Relaying in Multi-User Massive MIMO IoT Systems. 2024 IEEE International Conference on Communications Workshops (ICC Workshops), 529–534. doi:10.1109/iccworkshops59551.2024.10615968.

[39] Li, B., Zhao, S., Zhang, R., & Yang, L. (2021). Full-Duplex UAV Relaying for Multiple User Pairs. IEEE Internet of Things Journal, 8(6), 4657–4667. doi:10.1109/JIOT.2020.3027621.

[40] Zakia, I. (2019). Maximizing the Sum Rate of Massive MIMO with Rectangular Planar Array and MRT Beamforming. 2019 IEEE 89th Vehicular Technology Conference (VTC2019-Spring), 1–5. doi:10.1109/vtcspring.2019.8746334.

[41] Palomar, D. P., & Chiang, M. (2006). A tutorial on decomposition methods for network utility maximization. IEEE Journal on Selected Areas in Communications, 24(8), 1439–1451. doi:10.1109/JSAC.2006.879350.

[42] Zeng, Y., Zhang, R., & Lim, T. J. (2016). Wireless communications with unmanned aerial vehicles: Opportunities and challenges. IEEE Communications Magazine, 54(5), 36–42. doi:10.1109/MCOM.2016.7470933.

[43] Mozaffari, M., Saad, W., Bennis, M., & Debbah, M. (2016). Efficient Deployment of Multiple Unmanned Aerial Vehicles for Optimal Wireless Coverage. IEEE Communications Letters, 20(8), 1647–1650. doi:10.1109/LCOMM.2016.2578312.

[44] Wu, Q., Zeng, Y., & Zhang, R. (2018). Joint trajectory and communication design for multi-UAV enabled wireless networks. IEEE Transactions on Wireless Communications, 17(3), 2109–2121. doi:10.1109/TWC.2017.2789293.

[45] Pan, C., Ren, H., Wang, K., Xu, W., Elkashlan, M., Nallanathan, A., & Hanzo, L. (2020). Multicell MIMO Communications Relying on Intelligent Reflecting Surfaces. IEEE Transactions on Wireless Communications, 19(8), 5218–5233. doi:10.1109/TWC.2020.2990766.

[46] Sabharwal, A., Schniter, P., Guo, D., Bliss, D. W., Rangarajan, S., & Wichman, R. (2014). In-band full-duplex wireless: Challenges and opportunities. IEEE Journal on Selected Areas in Communications, 32(9), 1637–1652. doi:10.1109/JSAC.2014.2330193.

[47] Duarte, M., & Sabharwal, A. (2010). Full-duplex wireless communications using off-the-shelf radios: Feasibility and first results. Conference Record - Asilomar Conference on Signals, Systems and Computers (IEEE), 1558–1562. doi:10.1109/ACSSC.2010.5757799.

[48] Al-Hourani, A., Kandeepan, S., & Lardner, S. (2014). Optimal LAP altitude for maximum coverage. IEEE Wireless Communications Letters, 3(6), 569–572. doi:10.1109/LWC.2014.2342736.